



Assessment of early anthracycline-induced cardiotoxicity using segmental strain of cardiac magnetic resonance compared with global strain and functional parameters: an animal study

Jun-Qi Liu^{1#}, Qian-Feng Luo^{1#}, Wan-Yin Qi¹, Zheng-Yuan Xiao¹, Xiao-Yong Zhang², Yong-Shu Lan¹, Jing Chen¹

¹Department of Radiology, The Affiliated Hospital of Southwest Medical University, Luzhou, China; ²Department of Clinical Science, Philips Healthcare, Chengdu, China

Contributions: (I) Conception and design: JQ Liu, QF Luo, YS Lan, J Chen; (II) Administrative support: YS Lan, J Chen, XY Zhang; (III) Provision of study materials or patients: WY Qi, ZY Xiao; (IV) Collection and assembly of data: JQ Liu, QF Luo, WY Qi; (V) Data analysis and interpretation: JQ Liu, QF Luo, XY Zhang; (VI) Manuscript writing: All authors; (VII) Final approval of manuscript: All authors.

[#]These authors contributed equally to this work and should be considered as co-first authors.

Correspondence to: Jing Chen, MD, PhD; Yong-Shu Lan, MD. Department of Radiology, The Affiliated Hospital of Southwest Medical University, 25# Taiping Street, Luzhou 646000, China. Email: yzqdcj@126.com; lyblue2008@aliyun.com.

Background: The identification of anthracycline-induced cardiotoxicity holds significant importance in guiding subsequent treatment strategies, and recent research has demonstrated the efficacy of cardiac magnetic resonance (CMR) global strain analysis for its diagnosis. On the other hand, it is noteworthy that abnormal global myocardial strain may exhibit a temporal delay due to different cardiac movement in each segment of the left ventricle. To address this concern, this study aims to assess the diagnostic utility of CMR segmental strain analysis as an early detection method for cardiotoxicity.

Methods: A series of CMR scans were performed in 18 adult males New Zealand rabbits at baseline time (n=15), followed by scans at week 2 (n=15), week 4 (n=9), week 6 (n=6), and week 8 (n=5) after each week's anthracycline injection. Additionally, following each CMR scan, two to three rabbits were euthanized for pathological comparison. Cardiac functional parameters, global peak strain parameters, segmental peak strain parameters of the left ventricle, and the presence of myocardial cells damage were obtained. A mixed linear model was employed to obtain the earliest CMR diagnostic time. Receiver operating characteristic (ROC) analysis was performed to get the parameter threshold indicative of cardiotoxicity.

Results: The left ventricular ejection fraction decreased at week 8 (P=0.002). There were no statistical differences in global strain throughout the experiment period (P>0.05). Regarding segmental strain analysis, the peak segmental radial strain of the apical lateral wall exhibited a decrease starting from week 2 and reached its lowest point at this week (P=0.011). Conversely, peak segmental circumferential strain of the apical anterior wall showed an increase at week 2 and reached its peak at week 6 (P=0.026). The cutoff strain value by ROC analysis for these two walls were 46.285 and -16.920, with the respective areas under the curve (AUC) 0.593 [specificity =0.267, sensitivity =1.000, 95% confidence interval (CI): 0.471–0.777] and 0.764 (specificity =0.733, sensitivity =0.784, 95% CI: 0.511–0.816). Peak segmental longitudinal strain of the apical anterior and apical lateral wall showed relatively delayed changes, occurring in the 4th week (P=0.030 and P=0.048), the cutoff values for these strains were -12.415 and -15.960, with corresponding AUCs of 0.645 (specificity =0.333, sensitivity =0.955, 95% CI: 0.495–0.795) and 0.717 (specificity =0.433, sensitivity =0.955, 95% CI: 0.566–0.902), respectively. Notably, the myocardial injury was also observed at the corresponding periods.

Conclusions: Based on experimental evidence, the peak segmental strain of the apical lateral and anterior wall, as determined by CMR, demonstrated an earlier detection of anthracycline-induced cardiotoxicity compared to peak global strain and cardiac function.

Keywords: Cardiotoxicity; cardiac magnetic resonance (CMR); segmental strain; global strain; cardiac function

Submitted Dec 10, 2022. Accepted for publication Jun 28, 2023. Published online Jul 17, 2023.

doi: 10.21037/qims-22-1374

View this article at: <https://dx.doi.org/10.21037/qims-22-1374>

Introduction

As one of the most effective and widely used chemotherapeutic drug groups, anthracycline antibiotics are essentially cytotoxic drugs. While targeting cancer cells, such as these drugs also induce various adverse effects, including serious cardiotoxicity, ultimately resulting in heart failure (1-3). The 5-year survival rate of anthracycline-induced cardiomyopathy is less than 50% (4). As cardiotoxicity symptoms often manifest at a later stage, many patients undergoing chemotherapy experience difficulties in tolerating its relevant myocardial injury or cardiac dysfunction, thereby hindering their ability to complete the whole course of chemotherapy, which necessitates early monitor and timely intervention (5,6).

The assessment of left ventricular ejection fraction (LVEF) is often used to evaluate the potential or existing cardiotoxicity of in patients receiving chemotherapy for malignant tumors. However, assessment of LVEF is influenced by hemodynamic conditions and may not adequately capture early subtle alterations in left ventricular systolic function. Studies have reported myocardial injury can occur even in the presence of preserved ejection fraction (EF) (7,8). Strain assessment, whether through ultrasonic or magnetic resonance strain, may be a promising method to evaluate subclinical myocardial dysfunction and could monitor the acute, early, and late stages of cardiotoxicity (9-13). Specifically, the tissue tracking technology of cardiac magnetic resonance (CMR) has the potential to evaluate local or global myocardial dysfunction based on routine cine CMR images, offering better repeatability compared to ultrasonic strain, which is more convenient for monitoring and following up cardiotoxicity (14-16).

The focus of a study of cardiotoxicity with tissue tracking was the assessment of global peak myocardial strain, particularly global peak longitudinal strain (GPLS), as it has demonstrated predictive value in determining the occurrence of clinical events such as heart failure,

hospitalization, and death (16,17). However, it is important to acknowledge that cardiac movement differs among each segment of the left ventricle (LV), potentially resulting in a lag of global myocardial strain change. Consequently, segmental strain is expected to offer greater sensitivity than global strain, thus becoming an early method for cardiotoxicity detection. Moreover, several studies have found that patient prognosis does not improve based solely on global strain measurements (10), possibly due to the relatively delayed detection cardiac injury indicated by global strain analysis.

Therefore, the purpose of this study was to evaluate the value of segmental strain in the assessment of myocardial injury at various stages of anthracycline-induced cardiotoxicity in the rabbit model, which closely resembles the anatomical structure of humans (18), and to obtain the earliest sensitive CMR time and strain threshold for detecting cardiotoxicity, which may provide an effective and convenient monitoring method for chemotherapy patients. We present this article in accordance with the STARD and ARRIVE reporting checklists (available at <https://qims.amegroups.com/article/view/10.21037/qims-22-1374/rc>).

Methods

Animal model preparation

Experiments were performed under a project license (No. SWMU20210384) granted by Experimental Animal Ethics Committee of Southwest Medical University, in compliance with Southwest Medical University guidelines for the care and use of animals. A total of 18 rabbits (Adult male New Zealand white, weight: 2–3 kg, obtained from the professional animal center) were included, according to estimation of the smallest sample size and the unexpected losses. All rabbits were fed for 2 weeks to acclimatize to the environment in our dedicated animal laboratory (one rabbit in one cage, temperature 19–26 °C, humidity

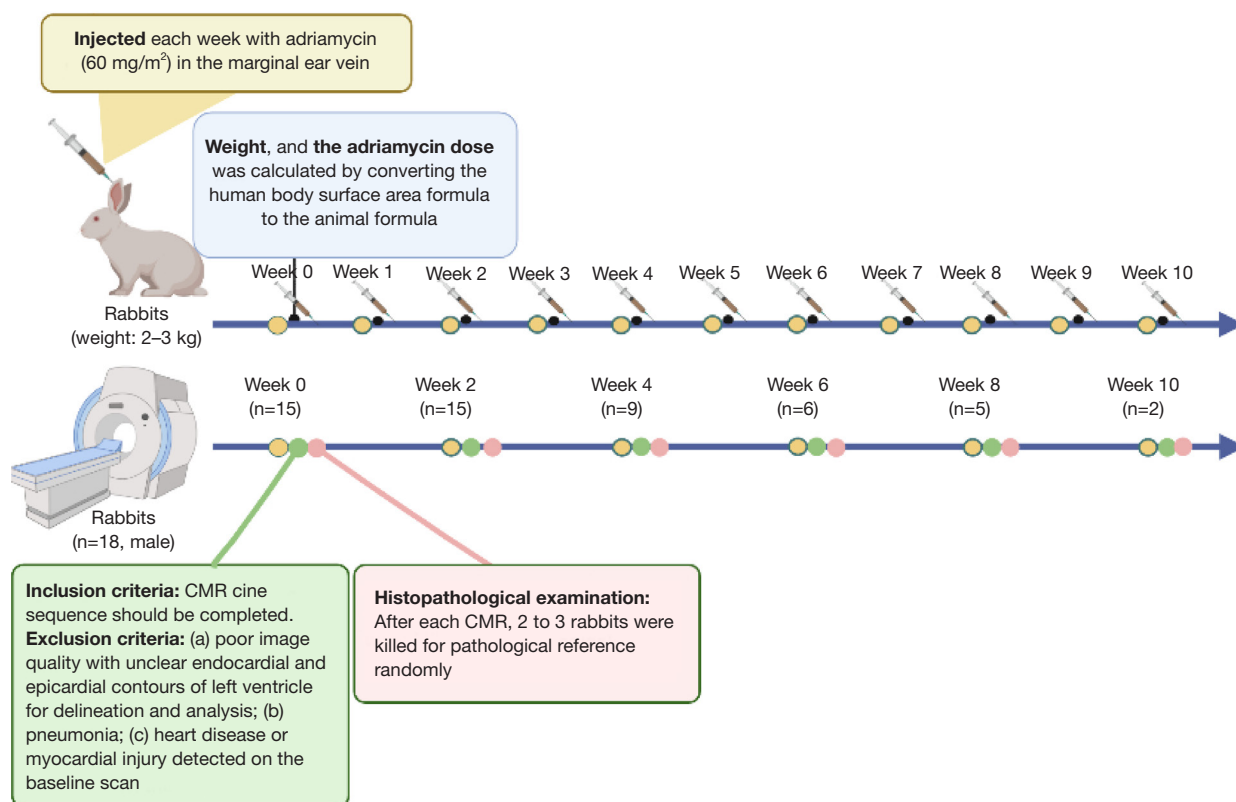


Figure 1 A flowchart of this study. The rabbits were injected each week with adriamycin and scanned every 2 weeks until they were sacrificed for histological study at the corresponding time points. The inclusion and exclusion criteria were applied to select rabbits with suitable CMR images for analysis, as indicated by the “n=” notation. Among the selected rabbits, three rabbits succumbed to anemia (n=1) and pulmonary infection (n=2) after completing the full CMR scan at the second week and were immediately subjected to pathological evaluation. This resulted in a total of 5 rabbits with pathological results, and one additional rabbit was excluded from the analysis due to inappropriate image quality. At the 6th week, 7 rabbits survived, out of which 6 rabbits had appropriate CMR image available for analysis, while 2 rabbits underwent pathological examination at this time point. CMR, cardiac magnetic resonance.

40–70%, regular feeding). Three rabbits were randomly selected and euthanized for baseline histological evaluation. The remaining fifteen rabbits underwent baseline CMR examinations before receiving weekly injections of adriamycin (60 mg/m²) in the marginal ear vein until they were sacrificed for histological study at the corresponding time points.

Based on the human dose of doxorubicin recommended by the Chinese Society of Clinical Oncology, the rabbit dose was calculated by converting the human body surface area (BSA) formula to the animal formula (19). In addition, CMR scans were performed 2 weeks after the first injection of adriamycin and were subsequently performed every 2 weeks until the completion of week 10. Following each

CMR scan, two to three rabbits were randomly selected and killed to serve as pathological reference at the corresponding time points. All rabbits were assigned unique identification numbers, and random number software was employed for the selection process. In cases where a selected rabbit had already died, another random number was generated until an available and viable rabbit number was obtained.

Inclusion criteria: CMR cine sequence should be completed. **Exclusion criteria:** (I) poor image quality resulting in unclear delineation and analysis of endocardial and epicardial contours of LV; (II) presence of pneumonia; (III) pre-existing heart disease or myocardial injury detecting during the baseline scan. Finally, 15 rabbits were included in this study (Figure 1).

Serial CMR scans

Preparation procedures before the CMR scan included soothing, heart rate reduction (using atenolol 1 mg/kg), continuous anesthesia (a mixture of oxygen and isoflurane), and electrocardiogram gating. Serial CMR scans were performed on a 1.5-T CMR scanner (Achieva, Philips Medical System, Netherlands). The standard segmented steady-state free-precession (SSFP) cine images were acquired at short-axis, two-, three-, and four-chamber long-axis views covering the whole LV to analyze cardiac function and strain. The following cine CMR parameters were used: echo time (TE) =1.84 ms, repetition time (TR) =3.7 ms, field of view =180 mm × 180 mm, matrix =144×144 pixels, slice thickness =5 mm, acquisition voxel size =1.67×1.67 mm², and recon voxel size =1.25×1.25 mm². Finally, 20–30 cardiac phases were acquired in a cardiac cycle for the rabbits.

Image analysis

Image analysis was conducted with special CMR post-processing software (Cvi42, version 5.12.4, circle cardiovascular imaging Inc., Calgary, Canada) by two experienced radiologists, each with over 3 years of expertise in CMR diagnosis. To assess the strain of the LV, a 16-segment model consistent with the American Heart Association model was used (20).

Myocardial cells consist of circular and longitudinal muscle fibers, each playing a distinct role in cardiac motion. Circular muscle fibers play a significant role in short-axis and circumferential motion, whereas longitudinal muscle fibers primarily drive movement in the long-axis direction (21). Thus, myocardial strain can occur in three spatial directions: longitudinal, circumferential, and radial. Longitudinal strain refers to the shortening of the myocardium along the long-axis, extending from the base to the apex. Radial strain is radially-directed myocardial deformation toward the center of the left ventricular cavity and indicates left ventricular thickening and thinning motion during the cardiac cycle. And circumferential strain denotes shortening of myocardial fiber along the circular perimeter of LV, as observed in a short-axis view (11).

Endocardial and epicardial contours were drawn manually at both end-diastole and end-systole in both short- and long-axis images (*Figure 2*). Subsequently, CVI software automatically outlined the contours throughout the whole cardiac cycle, allowing for editing and correction

of any inaccuracies. From the extracted contours, the strain parameters were automatically calculated from the corresponding strain curves. The global strain parameters primarily included global peak radial strain (GPRS), global peak circumferential strain (GPCS), and GPLS. The software also determined the segmental strain parameters of LV, dividing it into six zones at the basal level, six zones at the middle level, and four zones at the apical level. These segment parameters included segmental peak radial strain (SPRS), segmental peak circumferential strain (SPCS), and segmental peak longitudinal strain (SPLS). In addition, polar maps and curve graphs depicting the different strains were generated to provide a visual representation of the obtained data.

The left ventricular outflow tract was included in image acquisition to enable cardiac functional analysis of the LV. The assessment of left ventricular function encompassed various parameters, including end-diastolic volume (EDV), end-systolic volume (ESV), stroke volume (SV), cardiac output (CO), LVEF, left ventricular myocardial mass (LVMM), and their respective values corrected by BSA/body mass index (BMI).

The measurements were performed by the same observers after a 2-week interval to assess intra-observer variability. To ensure unbiased assessments, the observers were blinded to the rabbits' relevant information during the measurement process.

Histology analysis

Following euthanasia, each rabbit's whole heart was immediately removed. The heart was then cross-sectioned along the short axis at the middle ventricular level and fixed using 10% formalin. After appropriate processing, including dehydration and implantation, the resulting slice thickness was 5 μm. Then, hematoxylin and eosin (HE) staining and Sirius red staining were performed. Quantitative evaluation was performed using a digital histology slide scanner (Pannoramic 250, 3D Histech, Budapest, Hungary). Two experienced pathologists, each with 5 years of experience, analyzed the histological data. Myocardial injury was assessed based on the observation of vacuolation of the myocardial cells, the disorder of the myocardial tissue structure, and the changes in the myocardial cell shape using micrographs of the left ventricular septum and ventricular free wall corresponding to the same site on the CMR image. The criteria of myocardial injury were recorded according to previous studies (18,22). Additionally,

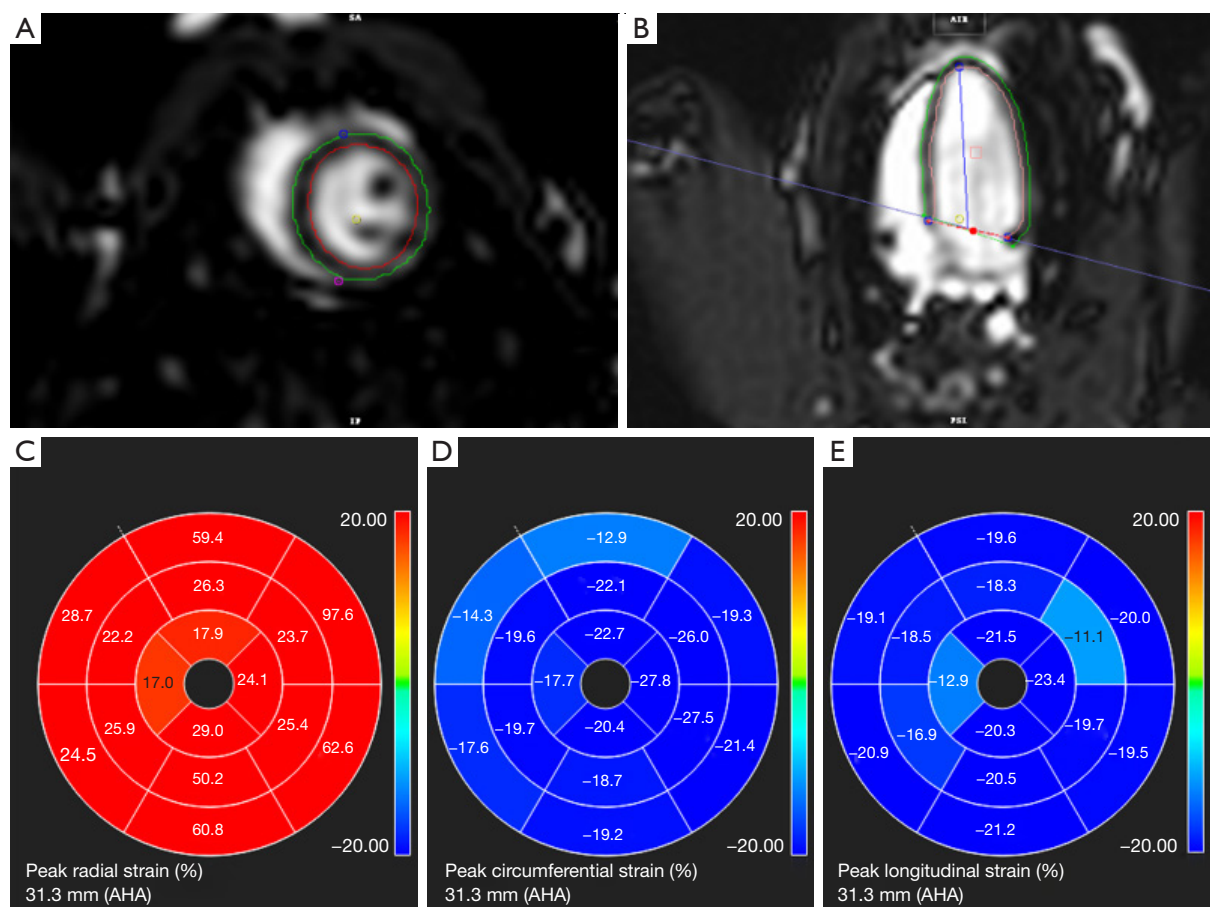


Figure 2 Schematic diagram illustrating the measurement of left ventricular strain. (A) Short-axis images of the left ventricle during systole. (B) Long-axis image of the left ventricle during systole. (C-E) Bull's-eye plot depicting the left ventricular strain at peak radial strain, peak circumferential strain, and peak longitudinal strain. AHA, American Heart Association.

collagen volume fractions (CVFs) were obtained by Sirius red staining. Regions of interest (ROIs) were manually drawn to calculate the CVFs in a Masson-stained slice corresponding to the CMR ROI areas in the midventricular LV septum myocardium.

Statistical analysis

All statistics were conducted using R software (R Core Team 2021, Version 4.1.2, Vienna, Austria). Normally distributed data were expressed as means \pm standard deviation, whereas continuous variables with a non-normal distribution were expressed as medians. To compare body weights between groups with different weeks, one-way analysis of variance (ANOVA) was used. For the comparison

of the cardiac function and strain parameters among different weeks, the linear mixed model was used to obtain the early sensitive CMR time for detecting cardiotoxicity. Additionally, receiver operating characteristic (ROC) curves were constructed based on the obtained time points and corresponding pathological results, the cutoff strain value with the best Youden's index, as well as sensitivity and specificity, were determined from the ROC analysis. And the area under the curve (AUC) was calculated to evaluate the diagnostic accuracy of the strain parameters for cardiotoxicity. A $P < 0.05$ was considered to be statistically significant. To assess intra- and inter-observer repeatability of measurements, intraclass correlation coefficients (ICCs) were used. ICCs greater than 0.8 indicated good consistency (23).

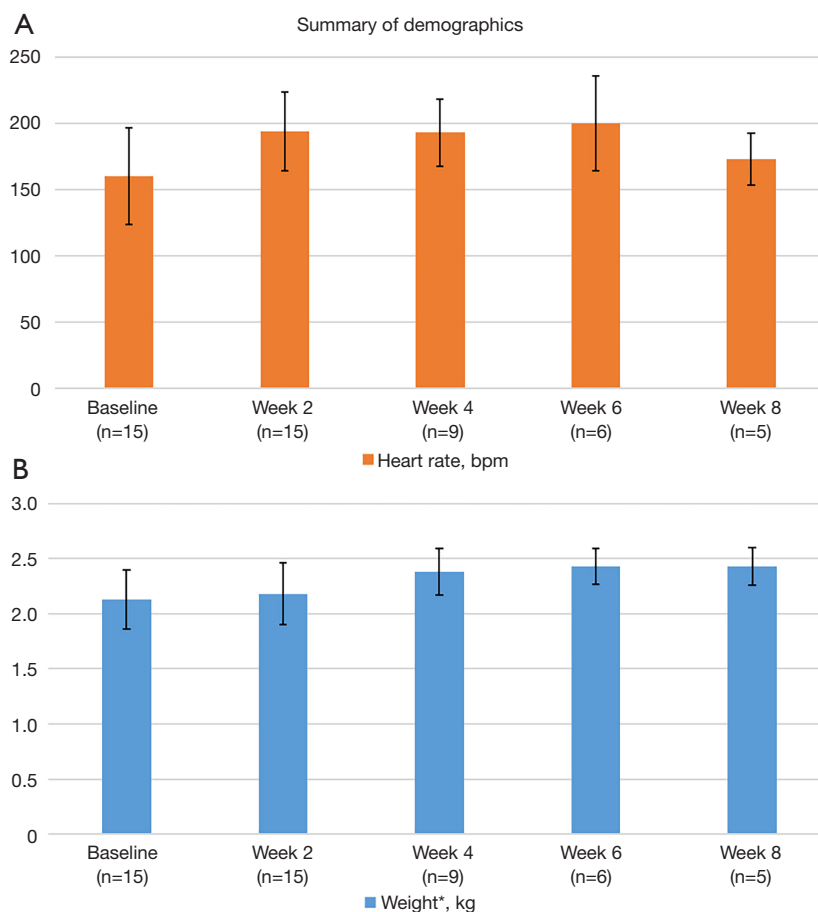


Figure 3 Summary of demographics of the heart rate and body weight. (A) Heart rate fluctuated within the range of 150 to 200 bpm. (B) The diagram indicates a slight increase in rabbit's weight as the model time points progress. Statistical analysis reveals a significant association between the increase in model time points and rabbit weight (*, $P=0.023$), suggesting a gradual weight gain over the course of the study. bpm, beats per minute.

Results

Animal clinical and pathological characteristics

Figure 3 lists the basic baseline and experimental modeling group information. The weights of rabbits showed a slight increase over time in the model group ($P=0.023$). Unfortunately, three rabbits died after completing the whole CMR scan, with one rabbit experiencing anemia and two rabbits developing pulmonary infections in the 2nd week. These rabbits were immediately dissected for pathological examination. Two additional rabbits were excluded from the analysis due to poor image quality at the 4th and 6th weeks, respectively. Only two rabbits survived for 10 weeks and

were not included in the statistical analysis.

The changing characteristics of the myocardial injury score and CVFs during the model period are shown in Figure 4. In the baseline group, the mean value of the myocardial injury score was 0 points, indicating no observable injury, and the mean CVF was 4.4%. The myocardial injury score reached its lowest value at week 2 (1 point), indicating mild injury, and increased gradually over time, reaching its highest value at week 10 (3 points), indicating more severe injury. Similarly, CVF exhibited the lowest value at week 2 (4.9%), and increased progressively, reaching its highest value at week 10 (23.4%), indicating increased deposition of collagen in the myocardium.

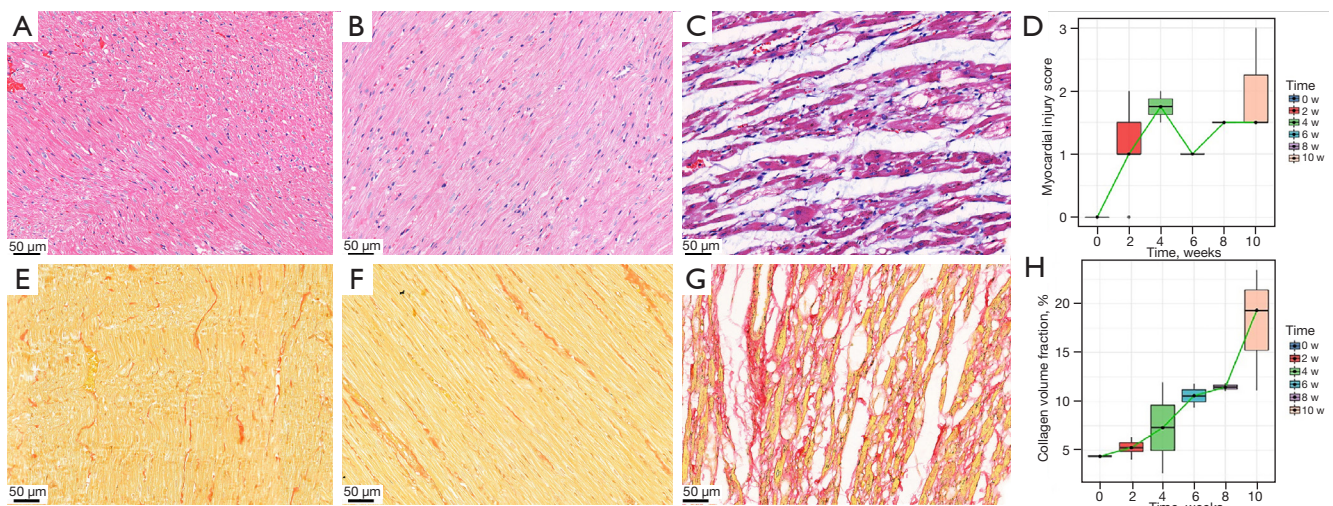


Figure 4 Histological findings of myocardial injury. (A) Normal myocardium from a control subject. HE staining; magnification $\times 200$. (B) Slight myocardial injury is visible in the LV septal wall of a 2-week model (myocardial injury score =1). HE staining; magnification $\times 200$. (C) Diffuse interstitial edema observed in the LV septal wall of a 10-week model (myocardial injury score =3). HE staining; magnification $\times 200$. (D) Box-plot illustrating the myocardial injury scores in different modeling time points. If the number of pathology was 2, the mean value was shown. If the number of pathology was more than 2, the median value was shown. The myocardial injury score was the lowest at week 2 (1 point) and the highest at week 10 (3 points). (E) Minimal collagen fibers observed in the interstitium of a baseline subject (measured CVF =4.4%). Picosirius red staining; original magnification $\times 200$. (F) No significant increase in collagen fibers was observed in a 2-week model (CVF =4.9%). Picosirius red staining; original magnification $\times 200$. (G) Abundant collagen deposition is visible in a 10-week model (CVF =19.3%). Picosirius red staining; original magnification $\times 200$. (H) Box-plot illustrating CVFs in different modeling time. If the number of pathology was 2, the mean value was shown. If the number of pathology was larger than 2, the median value was shown. The CVF was the lowest at week 2 (4.9%) and the highest at week 10 (23.4%). HE, hematoxylin and eosin; LV, left ventricular; w, week; CVF, collagen volume fraction.

LV function during different mode times

Left ventricular end-diastolic volume (LVEDV) and left ventricular end-systolic volume (LVESV) increased as early as week 4 ($P=0.034$ and $P=0.022$) and LVEF decreased at week 8 ($P=0.002$). Left ventricular cardiac output (LVCO) and left ventricle cardiac index (LVCI) increased at weeks 4 and 6 ($P=0.017$ and $P=0.009$), whereas LVSV increased at week 6 ($P=0.023$). LVMM increased at week 8 ($P=0.004$). No significant differences were observed in other cardiac function parameters at baseline, 2, 4, 6, or 8 weeks ($P>0.05$) (Table 1).

Left ventricular strain during different mode times

There were no significant differences in the LV global peak strain parameters at weeks 2, 4, 6, and 8 ($P>0.05$, Table 1). However, the segmental strain changed over the entire experimental period (Tables 2-4). The radial segmental strain

of the apical lateral wall for LV initially decreased at week 2 and reached the minimum at this time point ($P=0.011$, Table 2). Using ROC analysis, the cutoff value for radial segmental strain of the apical lateral wall to indicate cardiotoxicity was determined to be 46.285, with an AUC of 0.593 at week 2 [specificity =0.267, sensitivity =1.000, 95% confidence interval (CI): 0.471–0.777] based on the confirmation of the pathological results (Figure 5). The radial segmental strain of the mid-anterior wall was different at week 8 ($P=0.039$). The circumferential segmental strain of the apical anterior wall initially increased at week 2 and reached its maximum at week 6 ($P=0.026$, Table 3); its cutoff value for revealing cardiotoxicity at this point was -16.920 , with an AUC of 0.764 (specificity =0.733, sensitivity =0.784, 95% CI: 0.511–0.816) (Figure 5). The longitudinal segmental strain of the apical anterior and apical lateral walls increased at week 4 ($P=0.030$ and $P=0.048$, Table 4). The cutoff values for revealing cardiotoxicity were -12.415 and -15.960 , respectively. the corresponding areas under the

Table 1 Cardiac function and global peak strain parameters

Parameters	Baseline (n=15)	Week 2 (n=15)	Week 4 (n=9)	Week 6 (n=6)	Week 8 (n=5)	P value			
						Baseline vs. week 2	Baseline vs. week 4	Baseline vs. week 6	Baseline vs. week 8
EDV	3.77±0.53	3.69±0.80	4.41±0.75	4.89±0.79	5.04±0.98	0.844	0.034	0.003	0.003
ESV	1.86±0.30	1.89±0.48	2.30±0.38	2.59±0.45	2.90±0.57	0.659	0.022	0.002	<0.001
SV	1.90±0.31	1.80±0.39	2.11±0.43	2.30±0.36	2.14±0.50	0.826	0.128	0.023	0.216
EF	0.51±0.05	0.49±0.05	0.48±0.04	0.47±0.17	0.42±0.05	0.392	0.178	0.133	0.002
CO	0.31±0.08	0.35±0.10	0.40±0.04	0.45±0.05	0.37±0.07	0.194	0.017	0.002	0.216
CI	2.07±0.62	2.42±0.68	2.75±0.30	3.08±0.31	2.50±0.47	0.104	0.009	0.001	0.152
MM	1.49±0.33	1.44±0.23	1.48±0.35	1.60±0.31	1.95±0.31	0.930	0.814	0.262	0.004
HR	160.0±36.6	194.0±29.8	193.0±25.2	200.0±36.0	173.0±19.5	0.021	0.066	0.060	0.782
LV-GPRS	36.10±20.30	31.50±9.29	31.50±8.33	27.40±1.99	26.20±5.33	0.206	0.423	0.306	0.255
LV-GPCS	-16.00±3.57	-17.33±3.59	-16.56±3.66	-17.00±1.20	-16.36±3.45	0.247	0.795	0.342	0.515
LV-GPLS	-12.75±4.09	-11.96±2.97	-13.28±4.42	-11.53±1.75	-12.99±1.28	0.265	0.861	0.343	0.938

Values are means ± SD. EDV, end-diastolic volume; ESV, end-systolic volume; SV, stroke volume; EF, ejection fraction; CO, cardiac output; CI, cardiac index; MM, myocardial mass; HR, heart rate; LV, left ventricle; GPRS, global peak radial strain; GPCS, global peak circumferential strain; GPLS, global peak longitudinal strain; SD, standard deviation.

Table 2 Peak segmental radial strain parameters

Parameters	Baseline (n=15)	Week 2 (n=15)	Week 4 (n=9)	Week 6 (n=6)	Week 8 (n=5)	P value			
						Baseline vs. week 2	Baseline vs. week 4	Baseline vs. week 6	Baseline vs. week 8
AHA1	49.8±27.9	40.4±17.2	58.5±33.1	40.3±15.1	31.4±15.8	0.301	0.388	0.430	0.155
AHA2	35.9±21.5	33.7±16.1	37.4±23.4	34.8±14.4	24.0±8.7	0.780	0.780	0.964	0.240
AHA3	31.1±15.5	26.5±13.7	34.7±18.1	24.0±7.8	27.6±17.8	0.418	0.557	0.350	0.667
AHA4	36.3±16.0	24.3±26.5	41.3±18.7	22.7±8.9	37.4±20.5	0.503	0.559	0.180	0.913
AHA5	65.7±36.6	63.3±33.0	66.4±62.0	41.3±14.3	65.8±17.4	0.891	0.835	0.517	0.152
AHA6	61.5±45.9	58.2±26.7	58.1±50.0	50.7±12.1	48.6±24.2	0.902	0.829	0.870	0.956
AHA7	40.5±16.1	40.6±18.5	33.6±7.04	35.6±10.7	21.6±12.1	0.927	0.303	0.710	0.039
AHA8	34.2±16.5	36.5±13.0	26.9±10.0	31.6±7.4	27.9±7.7	0.484	0.214	0.788	0.634
AHA9	36.8±21.4	35.6±11.9	27.5±11.6	28.9±6.6	25.7±4.9	0.999	0.095	0.535	0.284
AHA10	38.8±37.3	32.6±16.1	35.2±15.5	26.2±6.8	36.4±15.5	0.916	0.682	0.507	0.451
AHA11	46.6±39.2	38.8±17.1	50.9±22.7	32.4±8.8	54.6±34.7	0.451	0.722	0.30	0.588
AHA12	57.7±44.3	44.0±17.0	54.5±15.9	43.0±25.1	25.0±19.4	0.196	0.966	0.492	0.082
AHA13	35.7±27.6	25.6±15.3	30.3±15.7	19.5±8.5	13.9±4.6	0.152	0.283	0.451	0.203
AHA14	33.0±21.3	26.7±15.6	23.7±13.4	25.3±13.8	18.6±8.1	0.063	0.226	0.314	0.055
AHA15	36.3±32.6	26.7±19.7	28.2±9.0	24.9±8.8	25.6±11.7	0.180	0.450	0.250	0.411
AHA16	40.1±31.3	25.6±18.9	27.9±9.9	26.0±8.7	27.7±10.9	0.011	0.557	0.302	0.540

Values are means ± SD. AHA1, basal anterior; AHA2, basal anteroseptal; AHA3, basal inferoseptal; AHA4, basal inferior; AHA5, basal inferolateral; AHA6, basal anterolateral; AHA7, mid anterior; AHA8, mid anteroseptal; AHA9, mid anteroseptal; AHA10, mid inferior; AHA11, mid inferolateral; AHA12, mid anterolateral; AHA13, apical anterior; AHA14, apical septal; AHA15, apical inferior; AHA16, apical lateral. AHA, American Heart Association; SD, standard deviation.

Table 3 Peak segmental circumferential strain parameters

Parameters	Baseline (n=15)	Week 2 (n=15)	Week 4 (n=9)	Week 6 (n=6)	Week 8 (n=5)	P value			
						Baseline vs. week 2	Baseline vs. week 4	Baseline vs. week 6	Baseline vs. week 8
AHA1	-16.50±4.77	-16.06±8.20	-11.45±9.48	-17.89±5.73	-10.96±7.25	0.868	0.114	0.696	0.154
AHA2	-15.65±11.50	-14.95±6.66	-10.37±9.93	-16.28±3.40	-14.04±4.10	0.865	0.169	0.848	0.753
AHA3	-17.10±6.59	-16.94±4.83	-14.53±9.34	-15.55±2.46	-17.58±2.85	0.798	0.341	0.470	0.998
AHA4	-12.02±9.84	-14.79±5.65	-8.51±16.10	-7.55±2.85	-13.73±2.80	0.371	0.369	0.301	0.695
AHA5	-19.50±6.64	-17.70±6.25	-13.36±8.12	-7.83±5.72	-14.68±4.88	0.668	0.051	0.003	0.540
AHA6	-18.19±11.90	-20.23±6.94	-15.53±8.30	-13.93±12.50	-14.65±4.98	0.561	0.502	0.412	0.542
AHA7	-19.40±3.76	-20.90±4.12	-21.46±3.47	-21.34±1.45	-18.15±6.39	0.312	0.232	0.321	0.550
AHA8	-17.29±10.00	-19.97±4.17	-19.51±4.55	-20.96±2.68	-17.63±3.11	0.526	0.587	0.160	0.882
AHA9	-13.58±11.80	-18.98±4.37	-15.90±5.11	-18.30±2.59	-17.37±2.31	0.127	0.690	0.135	0.219
AHA10	-11.24±11.40	-14.52±4.98	-15.37±6.12	-13.39±4.04	-13.99±3.77	0.179	0.536	0.622	0.339
AHA11	-17.10±4.86	-15.38±4.47	-17.45±3.95	-15.32±3.82	-16.21±3.61	0.223	0.951	0.532	0.903
AHA12	-19.93±4.32	-19.43±5.10	-21.49±2.79	-20.22±2.98	-19.63±3.91	0.747	0.388	0.889	0.889
AHA13	-12.41±12.40	-19.56±3.75	-20.76±3.60	-21.03±1.44	-16.98±5.13	0.026	0.008	0.094	0.221
AHA14	-11.60±16.80	-19.20±4.73	-15.77±5.65	-19.23±3.00	-16.29±4.23	0.023	0.543	0.080	0.512
AHA15	-16.24±6.04	-15.62±5.86	-16.29±11.10	-16.64±3.71	-19.44±4.87	0.807	0.987	0.907	0.381
AHA16	-19.47±4.99	-20.94±7.02	-24.06±1.78	-22.42±4.26	-25.10±4.99	0.457	0.053	0.261	0.053

Values are means ± SD. AHA1, basal anterior; AHA2, basal anteroseptal; AHA3, basal inferoseptal; AHA4, basal inferior; AHA5, basal inferolateral; AHA6, basal anterolateral; AHA7, mid anterior; AHA8, mid anteroseptal; AHA9, mid anteroseptal; AHA10, mid inferior; AHA11, mid inferolateral; AHA12, mid anterolateral; AHA13, apical anterior; AHA14, apical septal; AHA15, apical inferior; AHA16, apical lateral. AHA, American Heart Association; SD, standard deviation.

curve were 0.645 (specificity =0.333, sensitivity =0.955, 95% CI: 0.495–0.795) and 0.717 (specificity =0.433, sensitivity =0.955, 95% CI: 0.566–0.902), respectively (*Figure 5*).

Repeatability measurement

The inter-observer ICCs of GPRS/GPCS/GPLs for LV were 0.863, 0.886, and 0.906, respectively. And the intra-observer ICCs of GPRS/GPCS/GPLs for LV were 0.843, 0.844, and 0.876, respectively. Moreover, the inter-observer ICCs of SPRS/SPCS/SPLs for LV were 0.828, 0.837, and 0.843, respectively. And the intra-observer ICCs of SPRS/SPCS/SPLs for LV were 0.807, 0.815, and 0.823, respectively.

Discussion

The findings of this study based on New Zealand rabbits indicated that left ventricular segmental strain was more

sensitive than LVEF and left ventricular global strain for detecting early myocardial toxicity at the 2nd week of chemotherapy, which is earlier than the 16th week reported in another study (17). The apical lateral and apical anterior walls were identified as the most sensitive regions for assessing toxicity, suggesting that these segments can be focused on during screening for early cardiac toxicity. In addition, the study also identified the threshold parameters of segmental strain that can be used for the diagnosis of cardiotoxicity. Therefore, the CMR tissue tracking sequence with segmental strain, which has excellent repeatability and a convenient advantage, could be used as a potentially useful tool for the screening and follow-up of chemotherapy patients receiving anthracycline treatment.

Early detection of cardiotoxicity by segmental strain

The statement highlighted the limitation of relying solely

Table 4 Peak segmental longitudinal strain parameters

Parameters	Baseline (n=15)	Week 2 (n=15)	Week 4 (n=9)	Week 6 (n=6)	Week 8 (n=5)	P value			
						Baseline vs. week 2	Baseline vs. week 4	Baseline vs. week 6	Baseline vs. week 8
AHA1	-11.03±8.37	-11.30±3.61	-6.63±13.60	-6.98±8.39	-12.99±3.08	0.956	0.213	0.309	0.650
AHA2	-12.61±8.62	-11.95±3.35	-8.09±16.00	-8.49±4.27	-14.68±1.45	0.833	0.226	0.337	0.641
AHA3	-10.72±9.20	-11.42±6.32	-12.28±11.50	-10.29±1.72	-16.26±3.43	0.813	0.654	0.911	0.194
AHA4	-11.00±12.40	-13.28±7.02	-10.77±12.10	-13.24±2.99	-16.14±4.40	0.429	0.999	0.632	0.288
AHA5	-8.76±12.10	-10.86±6.10	-8.41±17.30	-11.91±3.86	-12.95±3.92	0.564	0.713	0.633	0.436
AHA6	-9.23±10.90	-8.32±8.81	-9.83±13.50	-9.31±3.62	-12.95±3.74	0.063	0.640	0.193	0.845
AHA7	-13.71±5.44	-9.56±9.62	-11.91±5.06	-10.33±2.20	-11.13±1.62	0.100	0.525	0.300	0.458
AHA8	-9.97±8.95	-10.09±8.69	-13.86±4.34	-12.65±1.65	-11.40±1.73	0.990	0.209	0.383	0.604
AHA9	-6.05±12.30	-10.20±5.21	-13.46±4.34	-11.36±2.33	-12.58±1.68	0.697	0.325	0.748	0.418
AHA10	-9.82±9.20	-10.57±6.50	-10.69±11.70	-10.31±2.54	-14.46±2.41	0.591	0.832	0.771	0.304
AHA11	-9.87±11.80	-11.43±5.38	-8.65±14.90	-9.61±3.65	-9.09±3.15	0.262	0.681	0.518	0.417
AHA12	-13.52±4.80	-10.58±5.39	-10.59±4.12	-9.00±2.75	-8.59±3.54	0.096	0.161	0.066	0.058
AHA13	-10.69±9.75	-14.65±3.36	-16.85±4.24	-16.41±1.42	-14.64±0.99	0.309	0.030	0.064	0.245
AHA14	-9.03±8.19	-9.50±3.01	-11.39±1.93	-10.85±2.59	-8.70±1.40	0.346	0.387	0.641	0.061
AHA15	-14.68±4.66	-14.18±3.56	-17.48±3.34	-13.79±2.04	-16.75±1.08	0.711	0.084	0.621	0.284
AHA16	-16.86±5.04	-16.11±4.43	-20.36±3.39	-18.25±1.71	-18.90±1.15	0.566	0.048	0.425	0.287

Values are means ± SD. AHA1, basal anterior; AHA2, basal anteroseptal; AHA3, basal inferoseptal; AHA4, basal inferior; AHA5, basal inferolateral; AHA6, basal anterolateral; AHA7, mid anterior; AHA8, mid anteroseptal; AHA9, mid anteroseptal; AHA10, mid inferior; AHA11, mid inferolateral; AHA12, mid anterolateral; AHA13, apical anterior; AHA14, apical septal; AHA15, apical inferior; AHA16, apical lateral. AHA, American Heart Association; SD, standard deviation.

on LVEF as a diagnostic parameter for myocardial injury of cardiotoxicity. A decrease in EF of more than 10% is considered indicative of myocardial injury, but usually progresses to an irreversible degree (24). And clinic symptom and time to presentation of cardiotoxicity are heterogeneous (8). Therefore, this parameter cannot be met by relying only on successive monitoring to judge myocardial injury (25). Consistent with our study, the cardiac function reaction time was too slow to respond to cardiotoxicity at week 8. This delay in detecting myocardial injury using EF alone may not effectively meet the clinical needs of chemotherapy patients, as irreversible damage may have already occurred by the time EF decreases significantly.

Left ventricular myocardial strain has been shown to be an earlier and more sensitive marker of contractile

dysfunction than LVEF alone (26). And the magnetic resonance strain based on tissue tracking technology, assuming that the measured deformation originates from the myocardium and that blood movement will not interfere with the process (11), had been reported to detect the occurrence and development of cardiotoxicity with GPLS as an independent predictor of a later reduction in LVEF (27). Moreover, the complex construction of left ventricular myocardium, with uninterrupted myocardial fibers emitting from the base and reflecting at the apex of the heart, and forming a closed “figure of eight” and eventually forming the endocardium and epicardium (28), contributes to the heterogeneous response of different myocardial segment to cardiotoxicity (29). The response of each segment may vary, with some segments exhibiting changes in strain earlier than others. This heterogeneity

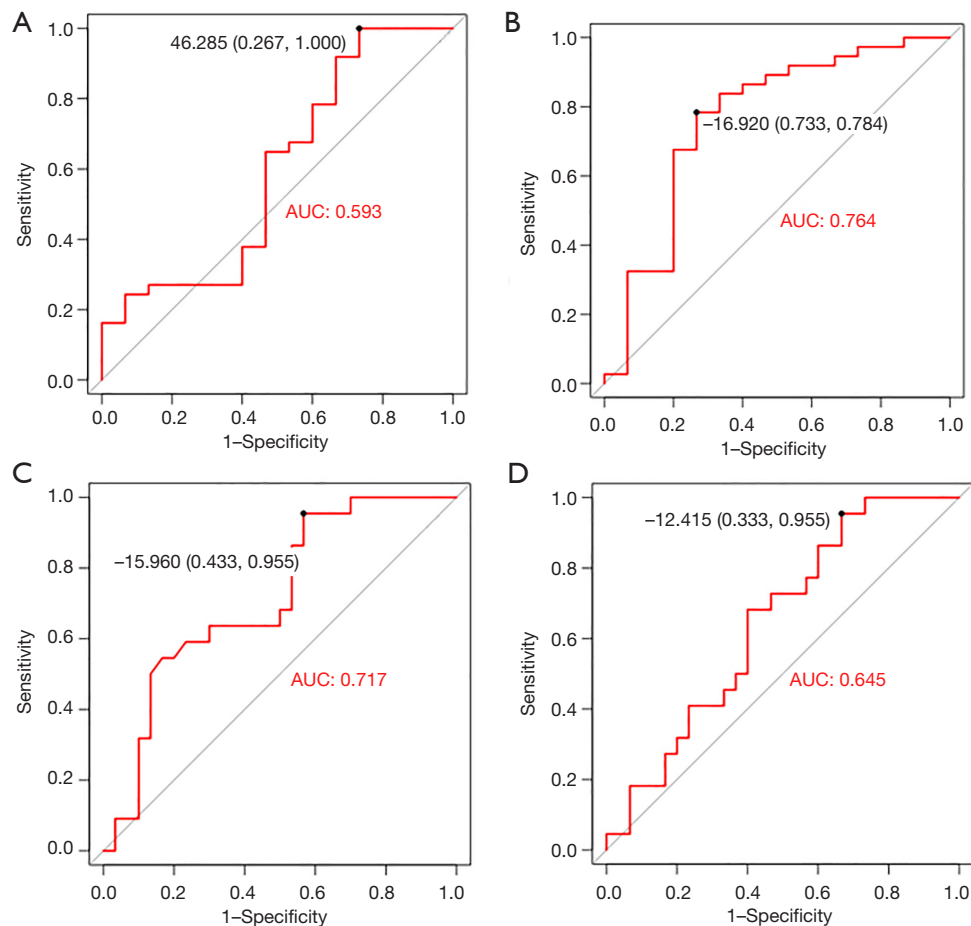


Figure 5 ROC curves for diagnosis. The AUC for AHA16 at week 2 in peak segmental radial strain was 0.593 (A). AUC for AHA13 at week 2 in peak segmental Circumferential Strain was 0.764 (B). AUC for AHA16 at week 4 in peak segmental longitudinal strain was 0.717 (C). AUC for AHA13 at week 4 in peak segmental longitudinal strain was 0.645 (D). AHA13, apical anterior; AHA16, apical lateral. ROC, receiver operating characteristic; AUC, area under the ROC curves; AHA, American Heart Association.

in the development of cardiotoxicity can result in delayed changes in global strain parameters, such as GPLS, which may not be significant until later stages of myocardial injury, like the results in our study.

Importantly, the study findings suggested that myocardial segmental strain, particularly in the apical anterior and apical lateral walls, can detect the occurrence of myocardial toxicity earlier in the 2nd week, aligning with the speculation regarding global strain. This observation is in line with the work of Anqi *et al.*, who proposed that the myocardium supplied by the left anterior descending artery may be more sensitive to the cardiac toxicity of anthracycline (30). Notably, the blood supply to the myocardium is primarily supplied by the coronary artery in diastole phase, and its power source is the diastolic pressure

of the aorta. It is known that distal blood vessels have lower pressure and slower blood flow velocity compared to proximal blood vessels. This characteristic may contribute to the accelerated absorption of anthracyclines in the myocardium. The apical anterior and apical lateral walls, which are supplied by the left anterior descending and left circumflex coronary arteries, respectively (20), may be particularly susceptible to anthracycline-induced myocardial injury. These two segments receive blood supply from locations farthest from the bend in the coronary artery's blood supply route. This anatomical arrangement may explain why myocardial injury due to anthracycline initially occurs in these specific myocardial segments, which can provide early detection and monitoring of cardiotoxicity in these vulnerable segments.

Diagnostic efficiency of the strain values with ROC analysis

The identification of an optimal screening time for early detection of cardiotoxicity using CMR has been achieved, but the onset of cardiotoxicity can vary among individuals. Consequently, the establishment of CMR parameter thresholds are necessary to effectively detect cardiotoxicity. Several studies have contributed to this area of research. Notably, Kammerlander *et al.* (7) found that tumor patients undergoing anthracycline chemotherapy were more prone to cardiac events when GPLS exceeded -8.5% . Similarly, Buss *et al.* (31) also proposed a comparable concept in the strain study of dilated cardiomyopathy. These studies support the importance of identifying specific CMR parameter thresholds to enhance the early detection of cardiotoxicity, thereby enabling timely intervention and management strategies.

While global strain in our study was not related to the results, segmental strain exhibited an early response to cardiotoxicity. To assess the diagnostic potential of segmental strain, we constructed the ROC curves and determined the cutoff values for different wall segments. Notably, SPCS of the apical anterior wall demonstrated excellent performance at week 2 of model time. When the cutoff value of -16.920 was reached, the corresponding AUC was 0.764, indicating a high level of specificity and sensitivity. Furthermore, the radial segmental strain of the apical lateral wall exhibited extremely high sensitivity, albeit with lower specificity, suggesting its potential as a promising marker for early screening of cardiotoxicity. It is important to note that these findings are based on an animal experiment and serve as a reference for future diagnostic and follow-up studies in clinical patients to detect cardiotoxicity in the early stage. And the application of these results to human subjects requires further investigation. In addition, the non-invasive and radiation-free nature of CMR makes it a valuable tool for long-term monitoring and follow-up of cardiotoxicity. By focusing on the apical anterior and the apical lateral walls, clinicians may be able to detect the occurrence of cardiotoxicity at an earlier stage, facilitating timely intervention and management in patients receiving anthracycline therapy.

This study had several limitations. Firstly, the sample size was relatively small, consisting of only 15 rabbits, which may limit the generalizability of the results. Conducting larger studies with a more substantial number of subjects would be beneficial to validate and further investigate the accuracy and reliability of this proposed approach. Secondly,

it is important to acknowledge that only male rabbits were used in this study, which was a deliberate choice to minimize potential confounding effects of female rabbit hormones. However, it is crucial to recognize the potential influence of gender-related factors in cardiotoxicity and consider their implications in future investigations. Lastly, the current work does not encompass risk stratification or differentiation between reversible and irreversible myocardial injury. Future studies should aim to incorporate pathological tissues analysis to enable comprehensive risk stratification using CMR and provide robust support for its clinical utility in this context.

Segmental strain analysis of CMR has demonstrated its potential in early screening and follow-up of anthracycline-induced cardiotoxicity, with detectability as early as the 2nd week of chemotherapy. Particularly, the assessment of peak segmental strain of the apical lateral and anterior walls appears to be promising. By utilizing CMR tissue tracking applied to conventional cine images, the severity of local LV myocardial deformation can be evaluated in patients. This approach offers high repeatability and stability, making it valuable for following up and early detection of cardiotoxicity in cancer patients receiving adriamycin treatment.

Acknowledgments

Funding: None.

Footnote

Reporting Checklist: The authors have completed the STARD and ARRIVE reporting checklists. Available at <https://qims.amegroups.com/article/view/10.21037/qims-22-1374/rc>

Conflicts of Interest: All authors have completed the ICMJE uniform disclosure form (available at <https://qims.amegroups.com/article/view/10.21037/qims-22-1374/coif>). XYZ is an employee of Philips Healthcare, which is not related to the current study. The other authors have no conflicts of interest to declare.

Ethical Statement: The authors are accountable for all aspects of the work in ensuring that questions related to the accuracy or integrity of any part of the work are appropriately investigated and resolved. Experiments were performed under a project license (No. SWMU20210384) granted by Experimental Animal Ethics Committee

of Southwest Medical University, in compliance with Southwest Medical University guidelines for the care and use of animals.

Open Access Statement: This is an Open Access article distributed in accordance with the Creative Commons Attribution-NonCommercial-NoDerivs 4.0 International License (CC BY-NC-ND 4.0), which permits the non-commercial replication and distribution of the article with the strict proviso that no changes or edits are made and the original work is properly cited (including links to both the formal publication through the relevant DOI and the license). See: <https://creativecommons.org/licenses/by-nc-nd/4.0/>.

References

1. Yu J, Wang C, Kong Q, Wu X, Lu JJ, Chen X. Recent progress in doxorubicin-induced cardiotoxicity and protective potential of natural products. *Phytomedicine* 2018;40:125-39.
2. Kremer LC, van Dalen EC, Offringa M, Ottenkamp J, Voûte PA. Anthracycline-induced clinical heart failure in a cohort of 607 children: long-term follow-up study. *J Clin Oncol* 2001;19:191-6.
3. Zhou Z, Wang R, Wang H, Liu Y, Lu D, Sun Z, Yang G, Xu L. Myocardial extracellular volume fraction quantification in an animal model of the doxorubicin-induced myocardial fibrosis: a synthetic hematocrit method using 3T cardiac magnetic resonance. *Quant Imaging Med Surg* 2021;11:510-20.
4. Felker GM, Thompson RE, Hare JM, Hruban RH, Clemetson DE, Howard DL, Baughman KL, Kasper EK. Underlying causes and long-term survival in patients with initially unexplained cardiomyopathy. *N Engl J Med* 2000;342:1077-84.
5. Cardinale D, Colombo A, Bacchiani G, Tedeschi I, Meroni CA, Veglia F, Civelli M, Lamantia G, Colombo N, Curigliano G, Fiorentini C, Cipolla CM. Early detection of anthracycline cardiotoxicity and improvement with heart failure therapy. *Circulation* 2015;131:1981-8.
6. Sawicki KT, Sala V, Prever L, Hirsch E, Ardehali H, Ghigo A. Preventing and Treating Anthracycline Cardiotoxicity: New Insights. *Annu Rev Pharmacol Toxicol* 2021;61:309-32.
7. Kammerlander AA, Donà C, Nitsche C, Koschutnik M, Schönbauer R, Duca F, Zotter-Tufaro C, Binder C, Aschauer S, Beitzke D, Loewe C, Hengstenberg C, Bonderman D, Mascherbauer J. Feature Tracking of Global Longitudinal Strain by Using Cardiovascular MRI Improves Risk Stratification in Heart Failure with Preserved Ejection Fraction. *Radiology* 2020;296:290-8.
8. Higgins AY, Arbune A, Soufer A, Ragheb E, Kwan JM, Lamy J, Henry M, Cuomo JR, Charifa A, Gallegos C, Hull S, Coviello JS, Bader AS, Peters DC, Huber S, Mojibian HR, Sinusas AJ, Kluger H, Baldassarre LA. Left ventricular myocardial strain and tissue characterization by cardiac magnetic resonance imaging in immune checkpoint inhibitor associated cardiotoxicity. *PLoS One* 2021;16:e0246764.
9. Ong G, Brezden-Masley C, Dhir V, Deva DP, Chan KKW, Chow CM, Thavendiranathan D, Haq R, Barfett JJ, Petrella TM, Connelly KA, Yan AT. Myocardial strain imaging by cardiac magnetic resonance for detection of subclinical myocardial dysfunction in breast cancer patients receiving trastuzumab and chemotherapy. *Int J Cardiol* 2018;261:228-33.
10. Houbois CP, Nolan M, Somerset E, Shalmon T, Esmailzadeh M, Lamacie MM, Amir E, Brezden-Masley C, Koch CA, Thevakumaran Y, Yan AT, Marwick TH, Wintersperger BJ, Thavendiranathan P. Serial Cardiovascular Magnetic Resonance Strain Measurements to Identify Cardiotoxicity in Breast Cancer: Comparison With Echocardiography. *JACC Cardiovasc Imaging* 2021;14:962-74.
11. Scatteia A, Baritussio A, Bucciarelli-Ducci C. Strain imaging using cardiac magnetic resonance. *Heart Fail Rev* 2017;22:465-76.
12. Thavendiranathan P, Negishi T, Somerset E, Negishi K, Penicka M, Lemieux J, Aakhus S, Miyazaki S, Shirazi M, Galderisi M, Marwick TH; SUCCOUR Investigators. Strain-Guided Management of Potentially Cardiotoxic Cancer Therapy. *J Am Coll Cardiol* 2021;77:392-401.
13. Egashira K, Sueta D, Tomiguchi M, Kidoh M, Oda S, Usuku H, et al. Cardiac computed tomography-derived extracellular volume fraction in late anthracycline-induced cardiotoxicity. *Int J Cardiol Heart Vasc* 2021;34:100797.
14. Luetkens JA, Schlesinger-Irsch U, Kuetting DL, Dabir D, Homsy R, Doerner J, Schmeel FC, Fimmers R, Sprinkart AM, Naehle CP, Schild HH, Thomas D. Feature-tracking myocardial strain analysis in acute myocarditis: diagnostic value and association with myocardial oedema. *Eur Radiol* 2017;27:4661-71.
15. von Knobelsdorff-Brenkenhoff F, Schunke T, Reiter S, Scheck R, Höfling B, Pilz G. Influence of contrast agent and spatial resolution on myocardial strain results using feature tracking MRI. *Eur Radiol* 2020;30:6099-108.
16. Fischer K, Obrist SJ, Erne SA, Stark AW, Marggraf M,

- Kaneko K, Guensch DP, Huber AT, Greulich S, Aghayev A, Steigner M, Blankstein R, Kwong RY, Gräni C. Feature Tracking Myocardial Strain Incrementally Improves Prognostication in Myocarditis Beyond Traditional CMR Imaging Features. *JACC Cardiovasc Imaging* 2020;13:1891-901.
17. Wang R, Zhou Z, Schoepf UJ, Varga-Szemes A, Strigenz A, Wang H, Liu Y, Xu L. Monitoring of anthracycline-induced myocardial injury using serial cardiac magnetic resonance: An animal study. *Int J Cardiol* 2021;328:111-6.
 18. Hong YJ, Park HS, Park JK, Han K, Park CH, Kim TK, Yoo SJ, Lee JY, Kim PK, Hur J, Lee HJ, Kim YJ, Suh YJ, Paek MY, Choi BW. Early Detection and Serial Monitoring of Anthracycline-Induced Cardiotoxicity Using T1-mapping Cardiac Magnetic Resonance Imaging: An Animal Study. *Sci Rep* 2017;7:2663.
 19. Jiang Z, Song E, Wang X, Wang H, Wang X, Wu J, et al. Guidelines of Chinese Society of Clinical Oncology (CSCO) on Diagnosis and Treatment of Breast Cancer (2020 version). *Transl Breast Cancer Res* 2020;1:27.
 20. Cerqueira MD, Weissman NJ, Dilsizian V, Jacobs AK, Kaul S, Laskey WK, Pennell DJ, Rumberger JA, Ryan T, Verani MS; American Heart Association Writing Group on Myocardial Segmentation and Registration for Cardiac Imaging. Standardized myocardial segmentation and nomenclature for tomographic imaging of the heart. A statement for healthcare professionals from the Cardiac Imaging Committee of the Council on Clinical Cardiology of the American Heart Association. *Circulation* 2002;105:539-42.
 21. Chen J, Yang ZG, Xu HY, Shi K, Guo YK. Assessment of left ventricular myocardial deformation by cardiac MRI strain imaging reveals myocardial dysfunction in patients with primary cardiac tumors. *Int J Cardiol* 2018;253:176-82.
 22. Lai RC, Wang XD, Zhang X, Lin WQ, Rong TH. Heart fatty acid-binding protein may not be an early biomarker for anthracycline-induced cardiotoxicity in rabbits. *Med Oncol* 2012;29:2303-8.
 23. Weltsch D, Chan CT, Mistovich RJ, Urwin JW, Gajewski CR, Fabricant PD, Lawrence JTR. Predicting Risk of Recurrent Patellofemoral Instability With Measurements of Extensor Mechanism Containment. *Am J Sports Med* 2021;49:706-12.
 24. Galán-Arriola C, Lobo M, Vílchez-Tschischke JP, López GJ, de Molina-Iracheta A, Pérez-Martínez C, Agüero J, Fernández-Jiménez R, Martín-García A, Oliver E, Villena-Gutierrez R, Pizarro G, Sánchez PL, Fuster V, Sánchez-González J, Ibanez B. Serial Magnetic Resonance Imaging to Identify Early Stages of Anthracycline-Induced Cardiotoxicity. *J Am Coll Cardiol* 2019;73:779-91.
 25. Čelutkienė J, Pudil R, López-Fernández T, Grapsa J, Nihoyannopoulos P, Bergler-Klein J, et al. Role of cardiovascular imaging in cancer patients receiving cardiotoxic therapies: a position statement on behalf of the Heart Failure Association (HFA), the European Association of Cardiovascular Imaging (EACVI) and the Cardio-Oncology Council of the European Society of Cardiology (ESC). *Eur J Heart Fail* 2020;22:1504-24.
 26. Huo H, Dai X, Li S, Zheng Y, Zhou J, Song Y, Liu S, Hou Y, Liu T. Diagnostic accuracy of cardiac magnetic resonance tissue tracking technology for differentiating between acute and chronic myocardial infarction. *Quant Imaging Med Surg* 2021;11:3070-81.
 27. Plana JC, Thavendiranathan P, Bucciarelli-Ducci C, Lancellotti P. Multi-Modality Imaging in the Assessment of Cardiovascular Toxicity in the Cancer Patient. *JACC Cardiovasc Imaging* 2018;11:1173-86.
 28. Torrent-Guasp F, Kocica MJ, Corno AF, Komeda M, Carreras-Costa F, Flotats A, Cosin-Aguillar J, Wen H. Towards new understanding of the heart structure and function. *Eur J Cardiothorac Surg* 2005;27:191-201.
 29. Chen J, Ding Y, Chen M, Gau J, Jen N, Nahal C, Tu S, Chen C, Zhou S, Chang CC, Lyu J, Xu X, Hsiai TK, Packard RRS. Displacement analysis of myocardial mechanical deformation (DIAMOND) reveals segmental susceptibility to doxorubicin-induced injury and regeneration. *JCI Insight* 2019;4:e125362.
 30. Anqi Y, Yu Z, Mingjun X, Xiaoli K, Mengmeng L, Fangfang L, Mei Z. Use of echocardiography to monitor myocardial damage during anthracycline chemotherapy. *Echocardiography* 2019;36:495-502.
 31. Buss SJ, Breuninger K, Lehrke S, Voss A, Galuschky C, Lossnitzer D, Andre F, Ehlermann P, Franke J, Taeger T, Frankenstein L, Steen H, Meder B, Giannitsis E, Katus HA, Korosoglou G. Assessment of myocardial deformation with cardiac magnetic resonance strain imaging improves risk stratification in patients with dilated cardiomyopathy. *Eur Heart J Cardiovasc Imaging* 2015;16:307-15.

Cite this article as: Liu JQ, Luo QF, Qi WY, Xiao ZY, Zhang XY, Lan YS, Chen J. Assessment of early anthracycline-induced cardiotoxicity using segmental strain of cardiac magnetic resonance compared with global strain and functional parameters: an animal study. *Quant Imaging Med Surg* 2023;13(9):5511-5524. doi: 10.21037/qims-22-1374